Thermal Characteristics of Lithium Indium Diselenide and Lithium Indium Gallium Diselenide Neutron Detection Crystals

A Thesis Presented for the
Master of Science
Degree
The University of Tennessee, Knoxville

Dustin Carroll Giltnane

May 2016

Acknowledgements

This research was funded in part by CNS Y-12 as part of their partnership with The University of Tennessee, Haslam College of Business. The sample synthesis was funded by Fisk University, Department of Life and Physical Sciences and Vanderbilt University, Department of Physics and Astronomy. The equipment was provided as a part of the Y-12 Plant Directed Research and Development Program.

Thank you to Dr. Howard Hall and Dr. Lawrence Heilbronn, the Master's Defense Oversight Committee members, for supporting this research and providing their advice and guidance. Thanks to my primary advisor Dr. Ashley Stowe for the time and dedication he has shown over the last year and half. Special thanks to my research group members, Maxx Jackson, Brenden Wiggins, Elan Herrera, Brittany Bennett, and Daniel Hamm. They made this body of work successful and contributed valuable time and effort above and beyond what was asked.

I would also like to acknowledge the time taken by Craig Dixon and Dale Hume from Thermtest Thermophysical Instruments for all their effort to aid not only my understanding of the TPS TC measurement technology but also the expected results of comparing pressed pellet to single crystalline materials.

Abstract

Tracking special nuclear materials (SNM) has never been more important than in the 21st century where information is transferred rapidly around the globe. Tracking SNM is important to nuclear power, weapons, medicine, and science. Neutron and gamma ray detection are the primary methods of detecting SNM. Increased movement and availability of SNM have increased the demand for radiation detection systems beyond the capacity of traditional neutron detection technologies (^{3}He) [Helium three]. Many alternative neutron detection materials are being considered, including $^{6}LiInSe_2$ [Lithium Indium Diselenide grown with lithium enriched in lithium six] and its derivative $^{6}LiIn_{1-x}Ga_xSe_2$ [Lithium Indium Gallium Diselenide: where the *x* represents varying concentrations of each constituent]. The research herein describes thermal transport and expansion properties of these materials to help better inform both crystal growers and detection designers. While preliminary reports indicate promising detection properties, improvements in crystal size and quality are required to improve neutron detection charge collection efficiency for nonproliferation applications.

Table of Contents

List of Tables

List of Figures

List of Equations

Chapter 1

Introduction and General Information

Neutrons are sub-atomic building blocks in the nuclei of atoms. They have no electronic charge and can travel relatively long distances through most materials. Therefore, stopping them in a material and detecting their presence is a technical challenge.

Nuclear weapons material, nuclear reactor fuel, and radioactive isotopes used in medical treatment naturally emit ionizing radiation. These materials can be used for both positive outcomes such as nuclear energy or nuclear medicine, but can also be used for nefarious acts. A key aspect to handling and using these materials is both tracking them and using their particle emissions to interrogate other materials. To this end, mankind has developed radiation detection devices. These devices observe and quantify ionizing radiation through a conversion reaction which produces a useable signal.

Increased detection requirements and ever changing detection or interdiction challenges force scientists to continually improve detection instrumentation. There are few suitable elements that react with ionizing radiation in a manner which can be used for detection purposes. Consequently, materials development is key to both improving technologies and meeting the growing demand. Additionally, it is of particular interest to have real-time, room temperature, hand-held detectors for facility interrogation and field surveys. To that end, many government agencies have increased their interest in promising neutron detection technologies.

Similarly, gamma ray detection techniques are useful because the presence of gamma rays of specific energies can confirm the presence of a particular isotope. This technique however, has one significant limitation. In the presence of a dense surrounding material such as lead, gamma ray attenuation can be significant. This can mask the gamma ray signatures of these special nuclear materials (SNM). Neutrons, on the other hand, easily penetrate dense and high atomic number materials. For heterogeneous or dense materials such as samples of metals, oxides, and nuclear waste, gamma ray attenuation is too high to permit accurate correction of the measured signal. Under these

circumstances, active and passive assay techniques based on neutron detection can significantly improve detection capabilities.

Neutron Detection Overview

Neutrons have the ability to travel long distances through common materials due to their electrically neutral nature; however, few materials readily release neutrons. They are only emitted when the nucleus is unstable and has more excess energy than that required to bind the neutron [1]. A material can emit neutrons through spontaneous fission, induced fission, or various nuclear reactions. Plutonium-239, a critical component of many nuclear weapons, is a primary example of a material that spontaneously fissions. Its detection is an essential science to homeland security and nuclear weapons non-proliferation [2]. Detecting neutrons can be used to identify, quantify, and/or qualify source materials.

The materials of interest in this study have shown promise in both neutron imaging and detection, making them ideal candidates for materials identification and investigation [3, 4].

Thermal Neutron Detection Overview

High energy neutrons are attenuated by collisions with the nucleus of atoms causing a decrease in their kinetic energy. The focus of this detection research lies with those neutrons that have undergone sufficient nuclear collisions to reduce their energy to the thermal regime. Thermal neutrons are defined as having an average kinetic energy of about 0.025 eV. [1] Finding materials that interact with neutrons can be difficult because all elements have a different probability of interacting with neutrons. This probability is quantified using the neutron scattering cross section [1].

Neutrons only interact with the nucleus of the atom. The interactions can either be an absorption, resulting in the neutron becoming a part of the atom with which it interacts, or a simple collision, where the neutron bounces off the nucleus and remains free until it loses enough energy to be absorbed. Certain isotopes will absorb neutrons and become unstable. The atom will return to stability by releasing some combination of particles in what is known as a nuclear reaction. It is important to note that not all

reactions are made equal. Some reactions emit a wide range of various particles with a wide range of energy. That variability of reaction products makes these reactions very hard to characterize. Fortunately, there are a limited number of materials that emit exactly the same particles with almost exactly the same energy every time. It is the nuclear reaction from these unique materials that are utilized for detection instrumentation.

Not all materials have the same probability of absorbing neutrons. That affinity is quantified as the neutron absorption cross-section. Therefore, in order to develop a neutron detector, one must focus on those materials that have the highest absorption cross-sections and whose interaction creates detectable particles. [1] Although the absorption cross section is an important factor when designing a detector, there are other considerations that must be taken into account. These could include but are not limited to reaction products, abundance, stability, cost, and ease of incorporation into a compound. Unfortunately, only a handful of materials have shown to be acceptable. The absorption cross-sections for materials of interest are given in Table 1 [5].

Table 1. Absorption Cross-section Comparison

Material	***Absorption Cross-section (barns)***
Boron-10	3,840
Helium-3	5,330
Lithium-6	940
Gadolinium-natural	49,700
Gadolinium-155	61,100
Gadolinium-157	259,000

Gadolinium is included in this table for symbolic purposes. The extremely high absorption cross section is not unique. Materials such as cadmium and uranium also have very high absorption cross sections but are not typically used for neutron detection because each of these elements produces a high gamma ray background. These gamma

rays can interfere with the signal and make source characterization difficult. Additionally, many of these materials are rare or difficult to work with. The other three materials are much more conducive to source characterization and in general, are not associated with the other difficulties. For that reason, we will focus on Helium, Boron, and Lithium for the remainder of the paper.

The high absorption cross-section of ^{3}He made it one of the dominant materials of choice for decades. Increased threat from terrorist attacks heightened the interest in tracking nuclear weapons, and thus the demand for ^{3}He has outgrown supply. [6] Helium is a noble gas, meaning it will not form a solid compound. This dictates that all helium based detectors be gas filled chambers of significant size. These problems have made an alternative detection material highly sought after.

The Boron-10 reaction is also a very popular vehicle for neutron detection. Unlike helium, it can be integrated into a solid or gaseous compound, enhancing portability and efficiency. It is also favorable from an availability and reaction products standpoint. Unfortunately, the ^{10}B neutron capture reaction produces a gamma ray 94% of the time. That gamma ray can make characterizing the incident radiation energy profile very difficult. Even still, recent technological advances have shown that large area, up to 16 cm^2, silicon diode based honey-comb style detectors can be used with relatively favorable efficiency. [7] As progress with boron based detectors continues it is anticipated that these detectors will be valuable for the future of neutron detection.

The Lithium-6 based reaction is of particular importance for its high reaction energy, *Q*-value, elemental abundance, and favorable reaction products. Although Lithium cannot be incorporated into a gas, investigations into ^{6}Li based detectors have yielded promising solid-state materials. Cs_2LiYCl_6: Ce (CLYC) and $LiInSe_2$ are two promising materials leading the way for the ^{6}Li based reaction. CLYC is a dual neutron/gamma scintillator which is much more mature material and is becoming commercially available, although without ^{6}Li isotopic enrichment. $LiInSe_2$ is unique in its ability to operate as both a scintillator and semiconductor and offers intrinsically high gamma transparency due to a low average Z-value. It is the first lithium based material to exhibit both traits [8].

Scintillator vs. Semiconductor Modes of Operation

Charged particles are needed to generate a usable signal in radiation detectors. In favorable detection mediums, charged particles are created as a result of instability after the nuclear reaction induced from neutron absorption. These particles liberate electrons or excite molecules within the crystalline lattice as they move through the material.

In semiconducting detection schema, electrons are driven through the material and can be collected on a cathode while the charge vacancy, hole, they left behind travel towards an anode by applying an electronic bias to the material. The amount of charge movement is measured by the quantity of liberated electrons and, under the right operating conditions, is directly proportional to the amount of energy deposited by the incident radiation [1]. Semiconductor-mode detection can only be efficiently accomplished by a material that readily conducts electrons through its structure.

A second method for extracting valuable information from incident radiation is known as scintillation. In this method, atoms within the material are excited by the transfer of kinetic energy from passing ions. Excited atoms promptly release this excess energy as photons when they return to their original state. The photons will be within the visible light spectrum if the energy gap between the excited and original state is optimized. This process is called fluorescence and materials that de-excite via this method are called scintillators. Photomultiplier electronics collect the scintillation light and produce a usable electronic signal. $LiInSe_2$ has been shown to produce usable particles through both scintillation and semi-conduction.

Chapter 2

Literature Review

This section is a technology comparison of detectors used in important real-world applications, giving context to the capabilities discussed for $LiInSe_2$. Situation suitability is a function of multiple characteristics that are created by the detection environment. Not all applications are relevant to this paper, even though the goal of the research is to create a high quality thermal neutron detector. For instance, thermal neutron detection can be used in any of the following:

1. Facility Investigation.
2. Neutron Detection in Extraterrestrial Locations.
3. Material identification in a controlled area.
4. Leak detection in power generating plants.
5. Portal monitoring at borders/shipping entries.

However, not all of these applications are favorable for small, portable, solid-state detectors. For instance, material identification in a controlled area can be done with very bulky, yet sophisticated systems such as high purity germanium cooled with a reservoir of liquid nitrogen. Additionally, portal monitoring requires large banks of detection arrays to investigation cargo containers. Therefore, compact detector designs are not favorable. The top three topics on the list are of interest for compact, solid-state detectors. The best detection systems for each of these applications will be discussed in the sections below.

Facility Investigation

Nuclear related facilities are regularly inspected to prevent unstable nations from developing nuclear weapons. Power plants are inspected to ensure all the material is accounted for and the facility is not operating with the intent to develop weapons grade materials. Facility inspections are completed with permanent equipment installed at the facility and mobile equipment used during visits. The systems are used together to monitor material movements and ascertain compositions.

Ideally, inspectors should be able to use portable devices during inspections to locate and identify radioactive sources. This requires a durable and portable detector with fairly high energy resolution. That detector could be passive or active depending on the goals of the operation.

Passive neutron detectors are used in these activities primarily to determine the mass of fissile plutonium in a sample. Active neutron detectors are used to initiate fission in uranium to determine the ^{235}U content, i.e. the enrichment. The current state of the art neutron detectors for facility interrogation are described in the following sections.

Passive Neutron Detectors for Facility Inspection

These detectors are used to detect spontaneous fission events in the even isotopes of plutonium. To accomplish this task, there are more than 15 different passive neutron detection systems regularly used by the IAEA [9]. There are generally two geometric configurations of passive neutron detectors used to inspect facilities. They include well detectors for samples small enough to fit within the detector and collar detectors that encircle samples too large for well detectors. Figure 1 provides visual representations of well and collar-type detectors. The majority of these systems use large arrays of ^{3}He proportional tubes and are not easily portable. Further, some have less than 20% detection efficiency. Even still, combinations of these detectors and sophisticated algorithms can determine the mass of plutonium in a sample to within 1% accuracy.

A small well coincidence counter is the standard for smaller sample applications. These detectors have been in use for years, yet they could definitely use improvement. The inventory sample counter is an example of a common portable neutron detector used in facility inspections. It has a high detection efficiency when compared to alternative neutron detection configurations of nearly 35%. Further, it is not hand-held and must operate in a controlled environment even though it is considered portable. Figure 2 is a common inventory sample counter. With modern electronics and computational processing, the detection medium is the limiting factor to creating a more compact alternative to this detection configuration.

Figure 1: a) Well-type neutron detection configuration. b) Collar-type passive neutron detection configuration[10]

Active Detection

Well and collar-type detection configurations are also used for active detection. These detectors generally have a detection head, housing the detection material and the neutron source. These systems are bulky and have limited portability, as with passive detection for facility inspection. A smaller alternative material would be very advantageous for both active and passive applications.

Neutron Detection in the Field

Many industries would benefit from the ability to detect fissile material with a portable unit while in the field. Many companies have begun developing portable neutron detectors to address the gap in the technology. The most promising detectors are based on boron carbide, Cs_2LiYCl_6: Ce (CLYC), LiF, or LiI. Additionally, BF_3 based proportional counter tubes have been created in a very portable configuration though they are not strictly hand held. The ability to discriminate against gamma rays is a very important feature for an advanced neutron detector.

Figure 2: Inventory sample counter [9]

Unfortunately, the ^{10}B neutron capture reaction produces a gamma ray 94% of the time. The energy carried by these gamma rays can become hidden in the background gamma field present when detecting SNM. Lost gamma ray energy makes characterizing incident radiation very difficult as the energy resolution becomes higher. For the comparison of advanced technologies, this section will focus on the lithium based devices.

Cs_2LiYCl_6: Ce (CLYC) Scintillator

This material was recently awarded $1 million in funding by the DHS to advance the research [11]. The research has enabled a commercially viable crystal that can be readily grown with a 2-inch diameter [12]. Current research is focused on the application of CLYC in various detector configurations in a range of applications.

CLYC has been optimized and current configurations show thermal neutron detection efficiency of 90% [13]. The light yield per thermal neutron absorption has been relatively low at about 20,000 photons [14]. It has also shown favorable gamma discrimination due to large variation in the rise time compared to neutrons, 13 ns for neutrons versus 40 ns with gamma rays [15]. The thermal neutron energy resolution has been enhanced to about 3.6%. It has also shown a gamma ray energy resolution of about 4% [16]. Simultaneous gamma and neutron detection with appreciable discrimination capabilities makes this material unique. Additionally, CLYC has shown a response to fast

neutrons [17], albeit with a much lower detection efficiency than thermal neutrons. Figure 3 is a visual representation of CLYC.

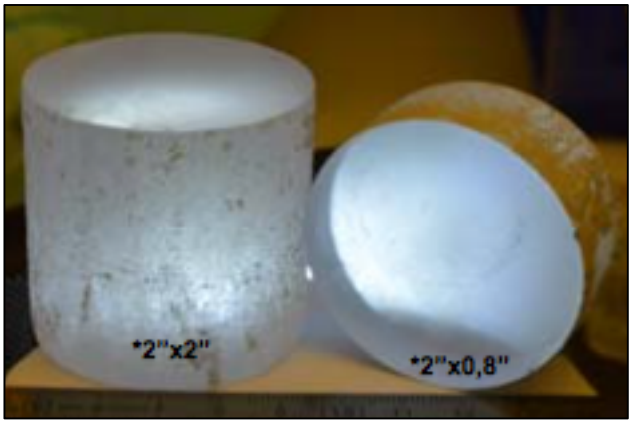

Figure 3: CLYC crystal

Other Lithium-based Scintillators

LiF based detectors having been commercially available for some number of years. They are well developed and there is little-to-no research on these detectors in the industry today. These detectors have not reached widespread use because of their inherent low neutron detection efficiency, sensitivity to gamma rays, and relatively low energy resolution. For instance nearly 25% on incident neutrons will back scatter out of the material before being absorbed [18]. Additionally, the chemistry of the material does not allow for a uniform medium after production. The result is a lattice of defects that the reaction products must traverse while depositing their energy. That inherent feature is a major factor giving the materials a poor energy resolution.

Lithium-iodide crystals have been in use for more than 60 years as thermal neutron detectors and the crystals are currently commercially available. There is little-to-no research being conducted to advance the material properties of LiI as with the other two lithium-based materials.

They are highly compact and can achieve very good detection efficiencies of thermal neutrons when coupled with efficient light collection technologies and advanced electronic processing. LiI crystals have also been used to detect gamma rays with an

energy resolution of about 8% [19]. Their gamma ray detecting capabilities are very similar to the better known NaI crystals. The only major handling difficulty is their extremely hygroscopic nature. The crystals come hermetically sealed and cannot be exposed to air or their properties will be degraded very quickly.

Neutron Detection in Extraterrestrial Locations

The major limiting factor to getting off the planet is size and weight. It is very expensive to send objects into space and therefore a small, solid state detector is optimal.

The material must be fairly durable as well to survive the potential turbulence of exiting the gravitational field and of landing on extraterrestrial bodies. It must also be able to withstand exposure to solar and background radiation. Additionally, it must be able to discriminate between the background radiation and the signatures from materials of interest. Accommodating these needs is a difficult task and the technologies available to conquer them are the same as those described for terrestrial neutron detection applications.

CLYC is the most promising and advanced technology previously discussed and has all the necessary capabilities to be a valuable neutron detector on extraterrestrial landscapes.

Neutron Detection Application Conclusions

A solid state neutron detection material would revolutionize many of the common neutron detection activities taking place across the globe. CLYC is the most promising material and exhibits many of the same capabilities of $LiInSe_2$ except it does not operate as a semiconductor. Either of these materials would have many of the same benefits for neutron detection that CdZnTe provided to gamma ray detection.

Chapter 3

Theory Supporting Research

History has shown difficulty in developing high quality materials that incorporate ^{6}Li. Traditional lithium based neutron detectors were created using material enriched in ^{6}Li surrounded by some semiconductor or incorporated in a compound, solid material. Early attempts to create materials with lithium in their regular stoichiometry have been successful [20], yet their application to neutron detection was not investigated. Over the last decade, great strides have been made to develop lithium containing chalcopyrite crystals. Additionally, they have shown promising results in response to thermal neutrons [4].

This section provides background on the work completed prior to the research detailed in this thesis. It is intended to give the reader context for the research and a better understanding of the strategy being used to perfect the detector material.

Early Work on $LiInSe_2$ as a Thermal Neutron Detector

Lithium-based chalcopyrite crystals were previously investigated for semiconductor applications in nonlinear optics as early as 1973 [21]. However, they were first investigated for use in radiation detection by Bell in 2005 [22]. Further advances were made over the next 10 years through the combined efforts of researchers at CNS Y-12 and The Universities of Tennessee, Vanderbilt and Fisk.

The efforts began by comparing the detection capabilities of $LiGaSe_2$, $LiInSe_2$, $LiInTe_2$, and $LiGaTe_2$ [23]. It is important to note that all initial work was focused on semiconductor operation, yet photoconductivity was measured and reported. These crystals showed variations in ease of growth as well as electron band gap. Previous work had reported $LiInSe_2$ to have a band gap within the optimum range for semiconductor operation at room temperature, which is between 1.8 and 2 eV [24]. The further research showed $LiInSe_2$ had the most promising band gap at 2.8 eV when defects were minimized, and exhibited the best growth by the vertical Bridgman method.

The results of that study identified $LiInSe_2$ as the best detector of alpha radiation and further investigation into neutron and gamma detection was conducted [25]. The

neutron detection research focused on natural lithium and optimizing the growth process to minimize previously seen voids, inclusions, and lattice defects. The crystals with natural lithium, approximately 7.5% ^{6}Li, showed a strong response to thermal neutrons and negligible response to fast neutrons as shown in Figure 4 below.

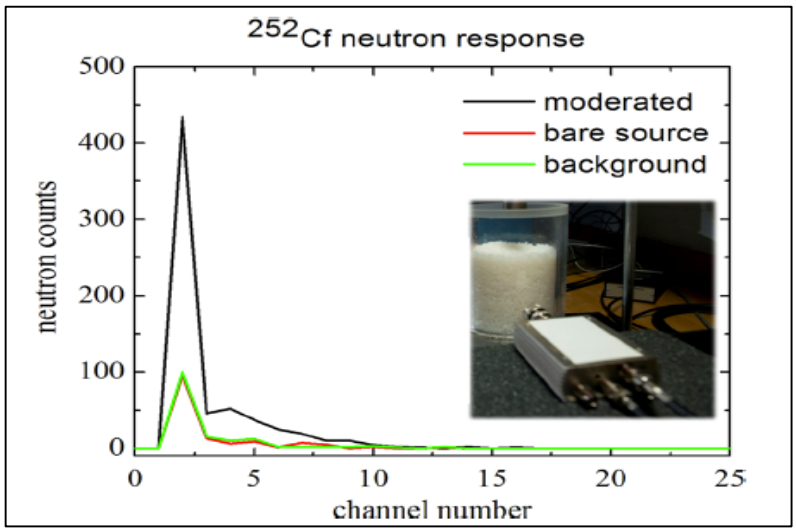

Figure 4: ^{nat}Li response to neutrons

This paper hypothesized the possibility of a much stronger response to thermal neutrons simply by increasing the thermal neutron absorption affinity of lithium. For instance, it was estimate that natural lithium only absorbed less than 25% of the incident neutrons, while crystals grown using enriched lithium would absorb nearly 82% of thermal neutrons. The remaining neutrons were hypothesized to be absorbed predominantly by indium, with a neutron absorption cross section of 194 barns. Unfortunately, the reaction products from thermal neutron absorption from indium are not usable in creating a signal. The next steps in development focused on $LiInS_2$ enriched in ^{6}Li.

Research on $LiInSe_2$ Enriched in ^{6}Li

Over the last three years $LiInSe_2$ has been grown and characterized using lithium enriched to 95% ^{6}Li. Measurements in both scintillator and semiconductor modes of

operation have been taken. Steps to understand crystallinity and material uniformity have simultaneously been executed to better understand the optimized material and growth processes.

Response to Thermal Neutrons in Semiconductor Operation

The two $LiInSe_2$ crystals used for neutron detection were red and yellow, with the assumption that color variations are caused by defects or variations in constituent concentration. The red crystals did not respond to thermal neutrons, while the yellow responded very well. It has been shown that the red crystals have higher concentrations of defects and charge trapping is likely the major reason for a lack of response [26].

Early thermal neutron measurements with $LiInSe_2$ enriched to 95% ^{6}Li showed a very strong response and promising detection efficiency of 66.1% [27]. Computational models in that research also noted the high contribution to neutron absorption contributed by ^{115}In. Figure 5 below gives a visual comparison of the thermal neutron absorption contribution of ^{6}Li versus the total $LiInSe_2$ crystal. Lukosi's work also indicates that the detection efficiency for a 5mm thick crystal is theoretically limited by ^{115}In to 81.2% versus 99.5% [28]. This identifies immediate room for improvement by replacing indium-115 with an element having lower neutron affinity.

Response to Thermal Neutrons in Scintillator Operation

Recent work has been focused on investigating $LiInSe_2$ for potential scintillation detection capabilities [8]. The neutron absorption of the material is still limited by the neutron affinity of ^{115}In as discussed for the semiconductor mode of operation. The materials response to both alpha and neutron particles was measured. A red and yellow crystal were used as well, with the red crystals performing poorly and the yellow having a favorable response. Interestingly, the results of this study show $LiInSe_2$ outperforming the CLYC crystal in decay time allowing for a faster response to incident radiation and thus less operational dead time during detection. The CLYC crystal was reported to have a decay time of 400 ns, while $LiInSe_2$ was shown to have a primary decay time split with 49% at ~32 ns and 51% at 149 ns [29]. $LiInSe_2$ had a scintillation light yield after corrections of approximately 3900 photons/MeV. This means every neutron induced reaction will create a usable light signature, considering the rather large reaction Q-value

of 4.78 MeV. Future work on scintillation should yield a high detection efficiency similar to that seen for semiconductor operation.

a) 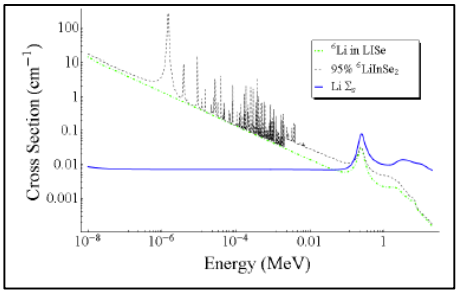

b) 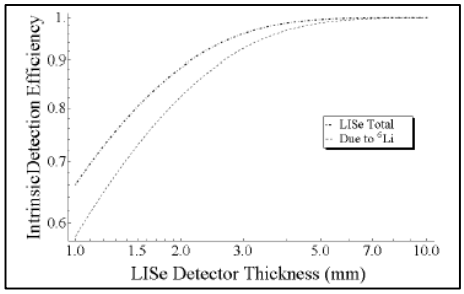

Figure 5: a) Macroscopic absorption and scattering neutron cross section for $LiInSe_2$ and ^6Li. b) First order detection efficiency for $LiInSe_2$ and ^6Li in $LiInSe_2$. [27]

Understanding Material Defects

The first step to optimizing $LiInSe_2$ is understanding the material properties preventing it from reaching theoretical performance. Recent work by two organizations using different analytical tools has been done to investigate material defects. Wiggins employed laser induced breakdown spectroscopy (LIBS) [26] while, Cui used photo-induced current transient spectroscopy (PICTS) and photoluminescence[30].

LIBS revealed inclusions in the crystal lattice that are closely correlated to both color and electron band gap variations. These defects include alkali and alkaline earth metals Na, K, and Ca. These metals are left over from the Li purification process and are carried through crystal growth to remain in the material. These impurities were found to be concentrated in the red regions of the crystal, agreeing with early investigations for non-linear optics applications. It was hypothesized by Wiggins that these impurity inclusions act as charge trapping sites, reducing electron hole mobility and thus lower detection efficiency.

LIBS analysis also revealed deviations from stoichiometry in the concentrations of Li and Se. Both materials have a relatively high vapor pressure and tend to evaporate during growth. It was shown that red regions of the crystal were Se deficient leaving excess Li and In. It is hypothesized that these deviations from stoichiometry are creating

additional charge trapping sites in red crystals. The combination of inclusions and deviations from stoichiometry could easily be causing the lack of performance seen in the red crystals.

The second organization also analyzed both red and yellow regions of $LiInSe_2$, yet they used PICTS. Their analysis focused on electron/hole mobility to identify charge mobility in various regions of the material. Their analysis showed the red crystals to be lithium rich as well and that annealing in a selenium atmosphere would turn the red crystals back to yellow. They were not able to identify exact material compositions of the defects but report six different types of defects all concentrated in the red regions of the crystal and related to deviations from stoichiometry. These defects include:

1. Lithium interstitials
2. Indium Vacancies
3. Lithium-on-indium antisites
4. Indium-on-lithium antisites
5. Selenium Vacancies
6. $XInSe_2$ (X is tentatively ascribed to Cu due to its low energy of formation.)

These defects all agree quite well with the results stated by Wiggins, with the exception of $CuInSe_2$. LIBS did not identify any Cu impurities in the red regions of the crystals.

Motivation for the Current Research Study

Existing Problems Preventing Potential Capabilities

Research into $LiInSe_2$ has revealed a promising material that could offer improvements over existing solid state neutron detector technology if its properties are perfected and performance nears theoretical. The parameters discussed above are displayed versus theoretical in Table 2 below.

The material defects within $^6LiInSe_2$ single crystals identified by Wiggins and Cui as well as the intrinsic material properties identified by Lukosi are preventing the current material from reaching its theoretical performance. The material is lacking in both charge carrier mobility and neutron absorption efficiency. Charge carrier mobility is inhibited by

material defects while neutron absorption efficiency is an inherent limitation of the existing material stoichiometry. The existing challenges are summarized in Table 3 below where theoretical numbers represent the reaction to thermal neutrons within a 5 mm thick crystal.

Table 2: Existing vs. Theoretical Capabilities

Metric	Current	Theoretical
Detection Efficiency	66.1%	99.5%
^{6}Li neutron absorption efficiency	82%	99.5%
Scintillation decay time	49% at ~32 ns / 51% at 149 ns	49% at ~32 ns / 51% at 149 ns

Table 3: Existing challenges of $^{6}LiInSe_2$

Challenge	Cause	Type of Problem
Low Thermal Neutron Absorption fraction from ^{6}Li	^{115}In within stoichiometry	Intrinsic material property
Ca, K, and Na Impurities	Byproducts of lithium enrichment	Material defect
Selenium deficient regions	Selenium evaporation during growth	Material defect
Lithium Interstitials	Excess Lithium	Material Defect

Eliminating the material defects will require greater understanding of material properties to improve growth. Changing intrinsic material properties will require modifications to the material composition. Theoretical pathways to solving these problems have been presented and are discussed below as motivation for this research.

Charge Carrier Mobility and Lifetime

The current state of the art material responds well to incident neutrons, yet has room for improvement. From the semiconductor perspective, energy resolution is a major area of concern with the material giving a continuum of energy across the full reaction *Q*

value [31]. It is likely that a lack of energy resolution is due to poor charge mobility and short charge carrier lifetime. It is common in compound semiconductors for charge mobility to be limited by defects in the crystal structure and impurities in material composition [32].

Previous work has shown these charge trapping sites to be precipitates of alkali and alkaline elemental earth impurities [26]. The impurities appear as point defects in an inhomogeneous spatial distribution. Their presence is shown to be correlated with a color shift from yellow to red. Additionally, charge trapping is being caused by interstitial atoms of excess lithium and indium caused by evaporation of selenium during the melt-growth process.

Material defects have been shown to be reduced through annealing. However, not all defects can be eliminated this way and it adds a secondary step to the production. Optimizing production should begin at the growth phase and thus that is where researchers have proposed beginning the corrective actions to eliminate material defects. Unfortunately, implementing changes to crystal growth practices can take many years because growing even a single crystal takes 3 months. Steps have been taken to speed up the process of improving growth in similar crystalline materials with computer simulations [33]. This process allows crystal growers to complete the same work in a matter of weeks that would previously have taken years. Even still, these simulations need to be as close to reality as possible to provide useful data.

Modeling research into similar semiconductor crystal growth has addressed material defects and sought mitigation methods [33]. The Vertical Bridgman growth method used in developing $LiInSe_2$ relies on very precise control of the material's temperature profile. Laminar flow is common place in Bridgman growth and can be affected by heat transfer through the bulk. Additionally, thermal gradients across the melt/solid interface have been shown to dramatically effect the pressure during crystal formation, causing cracking and bond breaking during solidification. Thus, the heat transfer behavior of the material is very important for optimizing crystal growth. These early models have been using an estimated single value for thermal conductivity based on

similar materials. The new data will allow growth modelers to use a polynomial to describe the thermal conductivity instead of a static number.

The heat capacity and thermal conductivity (TC) of $LiInSe_2$ had only been sparingly investigated prior to this study and that of $LiIn_{1-x}Ga_xSe_2$ had not been studied at all. Understanding the heat transfer properties of both materials will aid in perfecting their growth so that charge trapping can be mitigated.

Neutron Detection Efficiency

Theoretical models have shown a potential detection efficiency of 98.7% based purely on ^{6}Li absorption and subsequent reactions. Unfortunately, ^{115}In has a relatively high thermal neutron absorption cross section of 202 barns. It has been shown that ^{115}In constitutes 20% of the neutron absorption interactions in $LiInSe_2$ [28]. Therefore, $LiInSe_2$ is limited in its detection efficiency. This problem could be solved by substituting ^{115}In with Ga as described in original work exploring Li based ternary detection materials [34].

Adding Ga as a substitution material is a tricky process as it will also increase the valence electron band gap. The resulting material, $LiIn_{1-x}Ga_xSe_2$ will need to be optimized by finding the maximum detection efficiency as the band gap energy is increased and the fraction of thermal neutrons lost to ^{115}In reduced. Growing detector grade $LiIn_{1-x}Ga_xSe_2$ with varying compositions of Ga will require very advanced understanding of the material properties as with $LiInSe_2$. The thermal transport properties of $LiIn_{1-x}Ga_xSe_2$ have never been investigated and will be a critical component to growth.

Growing high quality crystals is the only way to ensure that the experimental results show a detection efficiency that is a function of changing the electron band gap and ^{115}In concentration. The first generation of $LiIn_{1-x}Ga_xSe_2$ crystals are being grown for experimental analysis. Unfortunately, they are difficult to grow and better material characterization is need to inform the process.

Thermal Conductivity to Improve Crystal Growth and Inform Detector Design

Growing these crystals relies on slow solidification of a bulk melt under precisely controlled temperature translational conditions. The temperature gradient across the

melt-solid interface is important to ensure a single nucleation event which can be propagated throughout the charge.

Local hot spots or cool points may occur due to differences in thermal expansion or thermal conduction which result in multiple grains, stresses, cracks, and impurity phase formation. Each inhibit the functional performance of the chalcopyrite crystal. Perfecting growth will maximize detection efficiency by minimizing charge trapping sites, ensuring free flow of charge carriers through the bulk material. Growth is a time intensive process, thus improvement by trial and error is costly and inefficient. Computational simulations, such as those currently used to develop CdZnTe [33], can dramatically reduce the number of growth cycles needed to perfect the process.

However, the simulation's effectiveness is dependent on the quality and extent of data describing material properties across the growth temperature regime. Current models are using static values for the TC instead of a dynamic function. The data collected herein shows that the TC of these materials changes dramatically with respect to temperature. Computational models can optimize crystal growth and improve detection efficiency with improved TC and the coefficient of linear thermal expansion (CLTE) data.

During normal detection operations, an electronic bias is applied to the crystal. That electronic bias coupled with radiation induced friction will elevate the temperate of the crystals. It is important for detection designers and operators to understand the TC of the crystal to prevent overheating during operation.

Coefficient of Linear Thermal Expansion to Inform Crystal Growth and Detector Design

During crystal growth the materials expand and contract as the thermal gradient is moved along the ampoule. The dimension changes cause stress in the material that could lead to fracture planes within the crystal. Understanding the stresses will help prevent unforeseen crystal fractures and lead to better crystal growth for eventual commercialization. Additionally, it will help detection engineers build an informed design with sufficient tolerance to account for material expansion while operating at various temperatures.

Chapter 4

Experimental

Materials Synthesis and Sample Preparation

The materials investigated include the following:

1. Single crystalline $LiInSe_2$
2. Pressed Pellet form crushed $LiInSe_2$
3. Single crystalline $LiGaSe_2$
4. Pressed pellet form of crushed $LiIn_{1-x}Ga_xSe_2$ where 5% of the indium has been replaced with gallium. The same material form of $LiIn_{1-x}Ga_xSe_2$ was used with 40%, 95%, and 100% indium replaced with gallium.

$LiInSe_2$ and $LiGaSe_2$ Crystals

All materials used in these experiments were sourced from FISK University and grown by Brenden Wiggins [8]. The crystals used for this experiment were grown by the Vertical Bridgman technique, which relies on slow solidification of a bulk melt under precisely controlled temperature translational conditions. Lithium was enriched to ~95% ^6Li for all samples. The crystals used in all experiments were not considered detector grade, but the bulk material properties are very similar to the detection grade. The $LiGaSe_2$ crystals began as optically semi-opaque and white, while the $LiInSe_2$ crystals were dark red.

The crystal samples were prepared for thermal conductivity from grown material as cylinders with a diameter of 16mm and a thickness of 9 mm. The 16 mm diameter was the size as grown, thus only the length dimension was changed. The flat sides were lightly polished until a smooth surface was achieved. No further material preparation was needed for thermal conductivity measurements.

For CLTE measurements, one of the cylindrical $LiInSe_2$ crystals was cut into a cube using a silicon carbide circular saw on a precisely controlled axial frame. The *x* and *y* axes were not determined; however, distinction of the *z* axis (direction of growth) was maintained by keeping that dimension visibly longer than the others. After the crystal was

cut, it was carefully cleaned and lightly polished. No other prep work was needed for these experiments.

$LiInSe_2$, $LiGaSe_2$, and $LiIn_{1-x}Ga_xSe_2$ Pressed Pellets Preparation

The pressed pellets of $LiInSe_2$ were made by crushing the crystals used in the previous experiment. A hydraulic press was used in conjunction with a precisely machined cylindrical dye. To maintain uniformity all pellets were pressed in air at a maximum pressure of 12,000 psi and held at 12,000 psi for 5 minutes. After pressing, the samples required no further preparation.

It is important to note that the $LiIn_{1-x}Ga_xSe_2$ crystals used to create the pellets with 5% and 40% In substitution were much higher quality than the 95% In substitution sample. The latter was much less uniform and had visible non-uniformities in material distribution. There were visible regions of black non-crystalline Ga powder within the sample. It is assumed that these concentrations of material would have some effect on bulk TC.

Experimental Methodology

$LiInSe_2$ and $LiGaSe_2$ both have a biaxial, orthorhombic crystal structure. The *z* axis was used on all thermal conductivity measurements. Single crystalline LiInSe2 was the only material whose coefficient of thermal expansion was characterized and all three axes were investigated.

Thermal Conductivity Measurements

The TC was measured through the transient plane source (TPS) method with the TPS 1500 system offered by Thermtest. In the TPS method a thin sensor containing two nickel circuits insulated by mica is placed between two samples of the material. One circuit contains a very tightly controlled Wheatstone bridge that adjusts to match and thus measure the circuit's electrical resistivity. The machine applies a very well-known voltage across the second circuit to induce material heating. The thermal coefficient of resistivity of nickel is very well known across the heating regime and is used to calculate the temperature of the sensor as the circuit is heated. The rate of heat transport away from the sensor, due to the TC of the samples, determines the temperature increase of the

sensor. The software program from TPS analyses the temperature change profile vs. time period exposed to heating power and calculates thermal conductivity. Nickel undergoes a curie transition between 300 and 420°C. Therefore, data taken in this temperature range is not useable.

The TC data was initially taken in multiple heating phases to ensure reliable data and structural integrity of the sensors. For instance, the first series of measurements were taken at room temperature under the same experimental conditions in five different instances. The same methodology was used on the first measurements taken across a thermal gradient, yet only repeated three times to establish confidence in the methodology. The experimental process was consolidated to a single heating sequence for each desired temperature regime after reliability of the measurements and experimental process was proven. Even still multiple data points were taken at each temperature for statistical confidence.

The TC of the $LiInSe_2$ single crystals was taken during both temperature increase and cool down to test changes in the material properties. The data was consistent when comparing heating and cooling phases. This process took nearly 12 hours, so all other data was only taken during temperature increase to save time.

The measurements were taken between RT and 700 °C for all but the $LiInSe_2$ single crystals. During the first high temperature investigations of $LiInSe_2$, the temperature was increased until the circuit within the sensor was destroyed, at 850 °C, with the last piece of fairly reliable data gathered at 800 °C. Unfortunately, at 800 °C deviations in the data were on the order of >15%. The other measurements were not taken above 700 °C due to the unreliability of the data. The mica insulation around the nickel circuit became very brittle after taking measurements at 700 °C. This made changing samples without destroying the sensor very difficult. For that reason, the extreme temperature range, > 400 °C, was investigated only after reliable data was taken at lower temperatures for each sample. That methodology helped minimize the number of sensors destroyed.

This process was repeated with the same material in pressed pellet form with average density at ~80% of the single crystal theoretical density. Upon repetition of the

pressed pellet measurements at temperatures above 300 °C, the TC increased. Heat transfer in materials is hindered by grain boundaries [35]. Thus the sample was likely becoming more single crystalline, reducing the grain boundary concentration. The literature on $LiInSe_2$ suggests that annealing at 500 °C turns red crystals yellow by removing defects within the crystalline lattice [26]. Therefore, it is likely that the TC was changing due to a similar annealing process happening during the course of the measurements, changing the structure of the material.

Crystals are grown at 940 °C and the TC measurements were to be taken up to 700 °C, or until sensor failure. The crystals were annealed at 800 °C for three hours to prevent annealing during measurements. The data became reliable after annealing, showing repeatability over multiple heating phases even after measurements at 700 °C. Additionally, the pellets were prone to cracking during experimental set up before annealing. After annealing the crystals were much more rigid and withstood the rigors of experimental setup, giving further credibility to annealing and an increase in crystallinity.

All experimental steps described for TC were repeated for $LiIn_{1-x}Ga_xSe_2$ pellets of previously described In/Ga concentrations up to 700 °C. The $LiGaSe_2$ single crystal samples were only measured up to 500 °C. Above 500 °C Se begins to evaporate off the surface of the crystal and these samples were required for further testing that dictated the need to maintain original material properties.

Thermal Coefficient of Linear Thermal Expansion and Normal Strain

The CLTE was calculated from data acquired using the Thermo-Mechanical Analyzer, model Q400, from TA instruments. This machine measures minute dimension changes in an oven over a specified temperature range using glass probes to maintain extreme precision. The intrinsic error of the system is stated as ± 0.1% while the temperature error is ± 1 °C. The data measured is the dimensional change along each axis of the crystal throughout the temperature range 25 - 500 °C. The data was exported from the TA instruments software into excel and Equation 1 was used to find CLTE.

$$CLTE = \frac{dx}{dTx_0} \ (x = length, T = temperature) \qquad \text{Equation 1}$$

Chapter 5

Results and Discussion

Thermal Conductivity

$LiInSe_2$ Crystals

$LiInSe_2$ is an anisotropic material with respect to crystallographic optics. For these experiments the TC was only measured in the *z* axis. Current literature on TC of $LiInSe_2$ has been published up to 70 °C [24].The results of that study give a TC at RT in the *z* direction of

$$K_z = 5.46 \pm 0.32 \text{ W/mK}$$

with a linear response to temperature described by (Temperature converted to °C for comparison):

$$K_z = 5.73 - 0.0105xT \qquad \text{Equation 2}$$

These results are very well aligned with our measurements represented by a TC at RT of

$$K_z = 5.42 \pm 0.27 \text{ W/mK}$$

and a linear correlation through 70 °C represented by:

$$K_z = 6.06 - 0.021xT \qquad \text{Equation 3}$$

These experiments extended their work to 800 °C. The error is reported as twice the standard deviation across all measurements. At 750 °C and 800 °C the error was 24% and 16% respectively. This is due to extreme temperature degrading the nickel circuit and difficulty obtaining quality data points. Each of these data points represents the average of only 2 measurements and thus the statistical certainty is not strong. They do follow the trend established at lower temperatures as can be seen in Figure 6 below. The relationship with respect to temperature through the full temperature range follows the polynomial:

$$K_z = 2\times10^{-5}T^2 - 0.0183T + 5.8197 \text{ } \textit{(T is temperature)} \qquad \text{Equation 4}$$

The TC drops off with temperature linearly until 300 °C where it begins to behave asymptotically. TC commonly decreases asymptotically with respect to temperature in crystalline semiconductors.

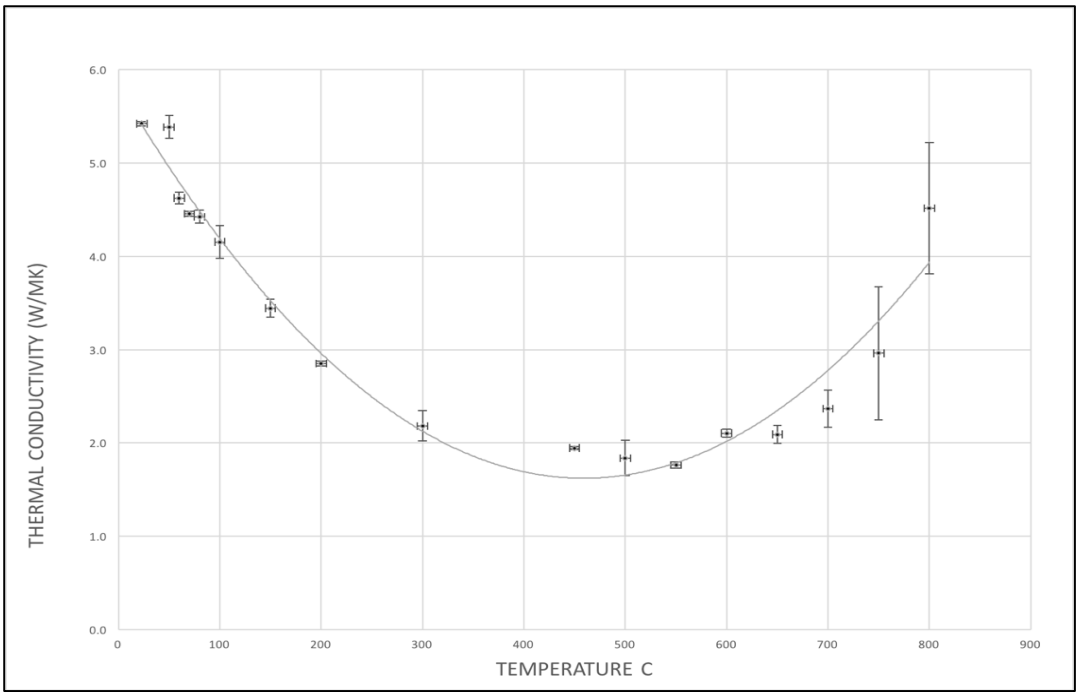

Figure 6: TC of $LiInSe_2$ crystals from 21℃ to 800℃

However, the increase starting at 550 °C is not commonplace. It reaches a minimum between 500 and 550 °C beyond which it begins an aggressive ascent back to its room temperature value. Heat is conducted in solids by charge carriers (electrons and holes), lattice waves (phonons), electromagnetic waves, spin waves, and random atomic excitations [35]. Lattice vibrational frequency increases with temperature to a maximum before atomic bonds are broken and atoms begin leaving their lattice sites. Selenium has been shown to begin breaking bonds between 450 and 550 °C. As the atoms move through the bulk they carry heat with them out of the material and thus increase the TC of the sample, creating the sharp increase we see above 550 °C. The trend seen in the data strongly correlates with both theory and known physical characteristics of the material.

Pressed Pellets

The pressed pellet TC was much lower than the single crystal as expected by theory and shown in Figure 7. As discussed in the experimental section the TC of the pellets was not repeatable during the first several heating sequences due to annealing during the measurements.

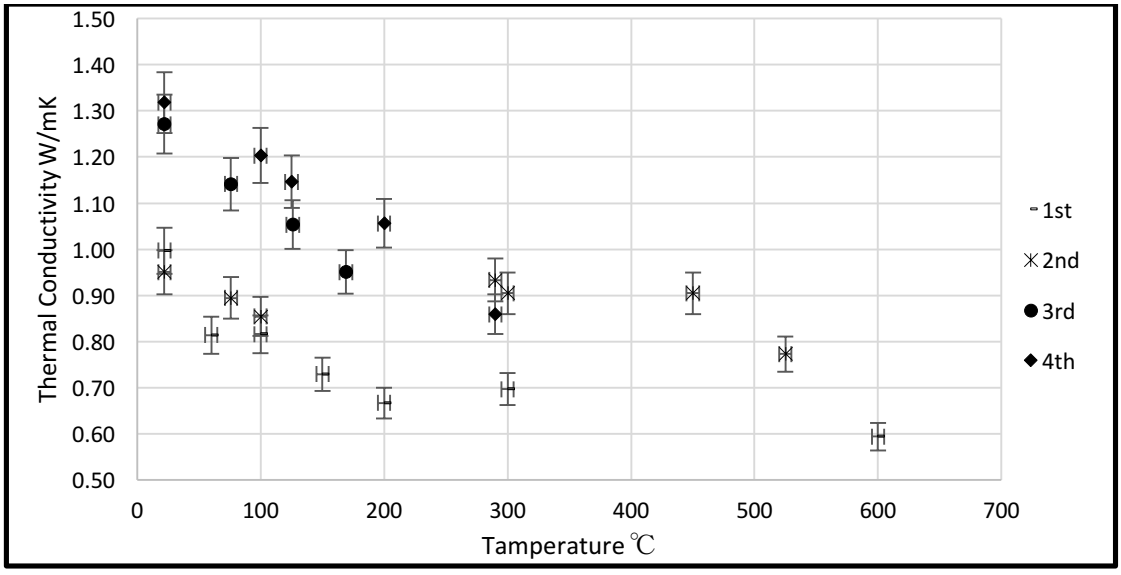

Figure 7: $LiInSe_2$ pellets before annealing. The legend denotes the number of heating sequence.

The pellets were annealed at 800°C, much higher than the intended measurement temperature, for three hours to prevent annealing during the measurement and establish repeatable data. The figure clearly shows that the TC of the pellets is steadily increasing each time the pellets were heated. The increase in TC is directly due to the ease of which phonons were traveling through the bulk material. The ease of phonon movement was increased from a reduction in grain boundaries from annealing. The error in these measurements calculated as twice the standard deviation of the measurements was much smaller than the 5% error stated in the operating parameters of the TPS 1500 manual. The vertical error bars represent the 5% accuracy of the machine and the horizontal error bars the 5°C variation of the furnace. After annealing the TC was retaken and that data is shown in Figure 8. The TC of the pellets after annealing is much higher than before and remained within 5% of the original through multiple heating sequences. The error bars for the pellets after annealing follows the same convention as before annealing. A comparison of the pre and post annealed pellet data is given in Figure 9. The comparison clearly shows a more uniform data set represented by the annealed crystals.

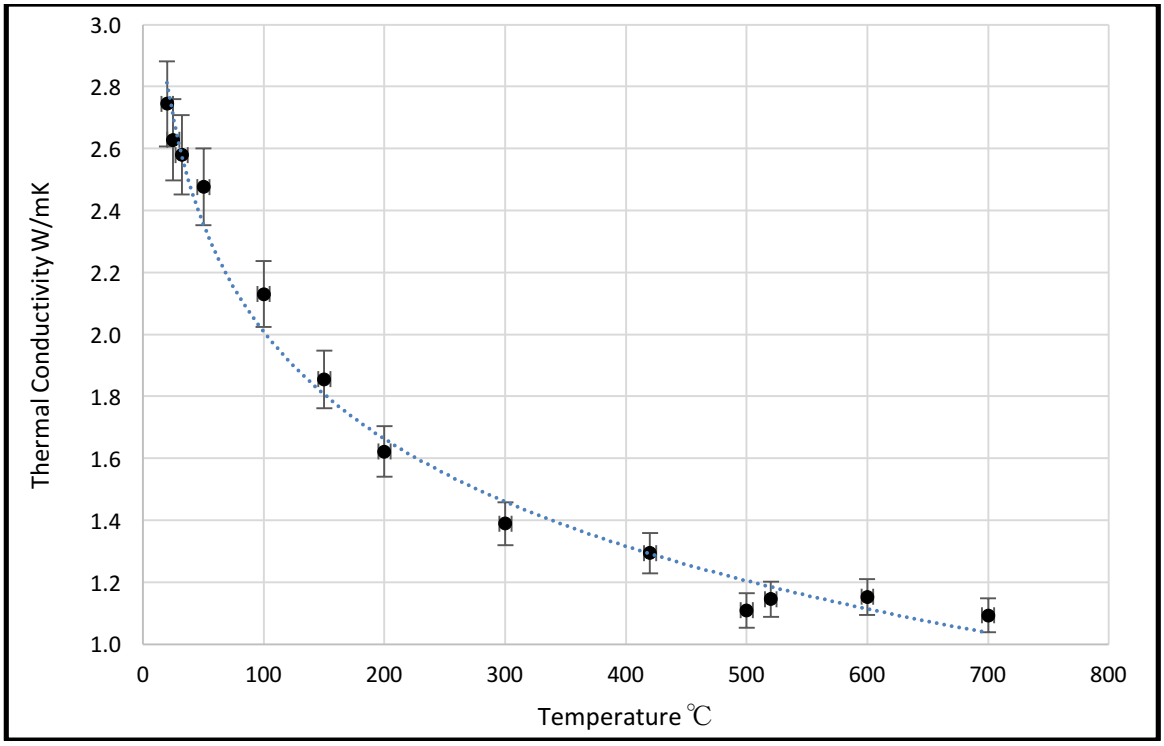

Figure 8: $LiInSe_2$ pellets after annealing

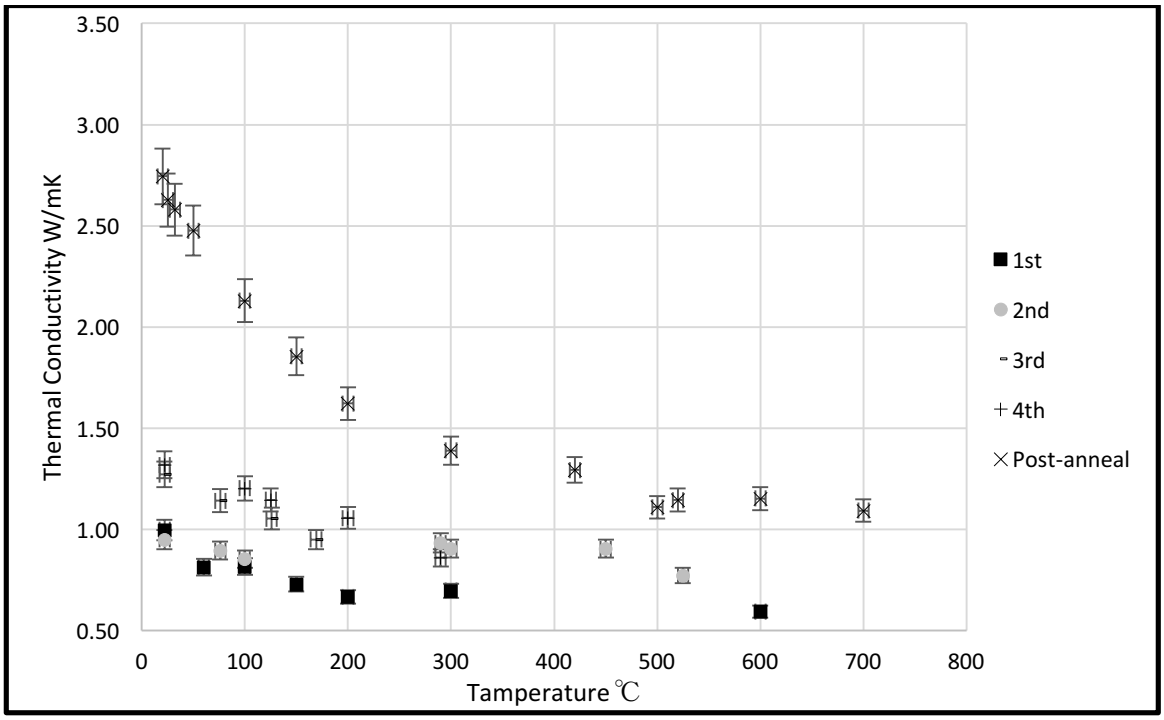

Figure 9: Pre vs. post anneal TC of the $LiInSe_2$ pellet

No literature has been found describing the TC of $LiInSe_2$ in pressed pellet form and it is assumed that this represents the first research on that topic. Figure 10 below is a comparison of the crystal TC and the post-anneal pellet TC.

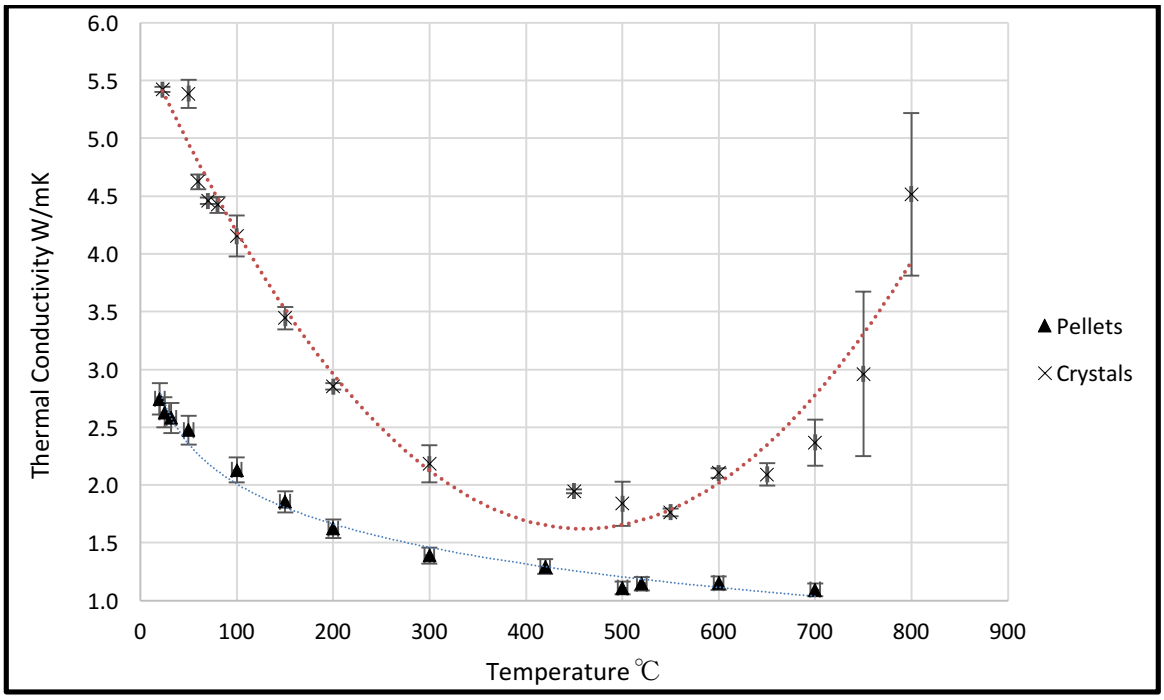

Figure 10: $LiInSe_2$ Crystal vs. annealed pellet TC

It is interesting to note that the crystal and annealed pellets follow the same general trend of aggressively decreasing TC through 300°C. The trends deviate from one another above 500°C where the crystal TC begins to increase and the pellets continue to decline. The increase in TC in the crystals was likely caused by atomic movements of selenium as it began to evaporate around 500°C. The powder form of the pellets did not prevent selenium from breaking away from its molecular bonds, but the densely pack grain boundaries would have greatly inhibited atomic movement. That inhibition could be preventing free atoms from moving through the material and causing them to remain in localized regions of the bulk. They are likely preventing phonon movement by their inability to travel through the material. This topic needs further investigation.

$LiGaSe_2$ Single Crystal Samples

$LiGaSe_2$ is an anisotropic material with respect to crystallographic optics. For these experiments the TC was only measured in the *z* axis. The temperature range only extended from room temperature to 500 °C to prevent Se off-gassing. This limit on temperature regime was intended to preserve stoichiometry so that further measurements of the optical properties could be made after this study was completed. The TC at room temperature was found to be 6.3 ± 0.3 W/mK. The only reference to the TC of $LiGaSe_2$ was found in a paper published by Isaenko et al [36]. In that paper the TC of $LiGaSe_2$ is estimated to be about 6.0 ± 0.2 W/mK based on published values and vibrational phonon modes of similar materials. It is encouraging that their study matches the results obtained in our experiments. The results of the measurements across the full temperature regime are given in Figure 11. The data follows the polynomial trend given in Equation 5.

$$K = 3E\text{-}05T^2 - 0.0213T + 6.6817 \qquad \text{Equation 5}$$

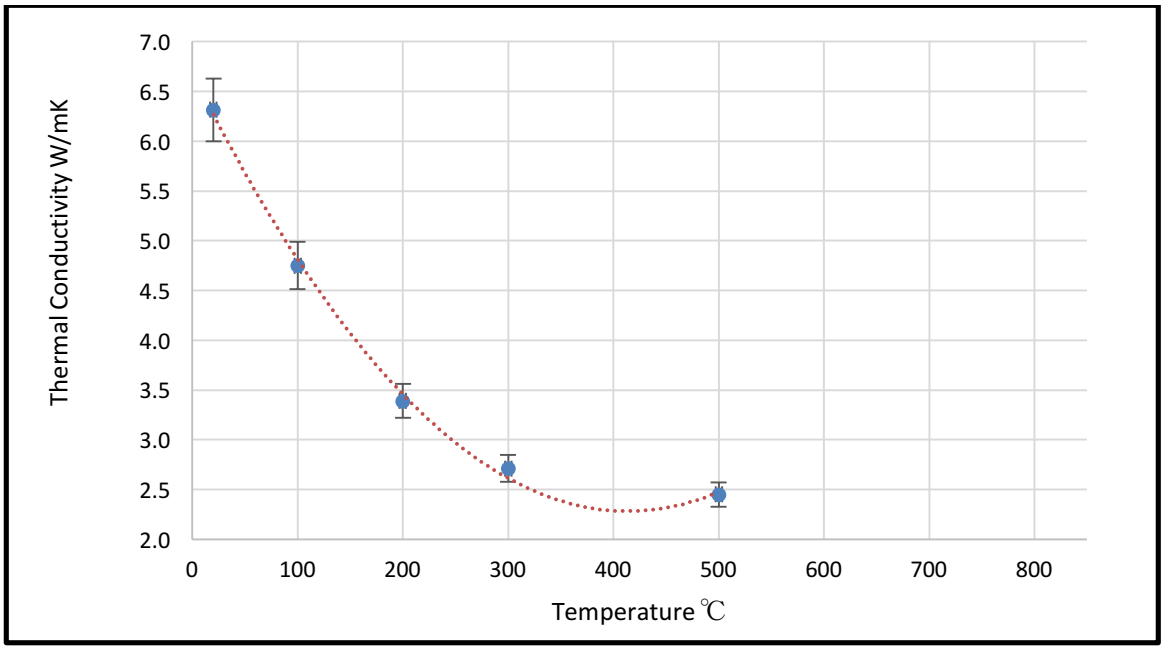

Figure 11: $LiGaSe_2$ vs. temperature

The data taken for $LiInSe_2$ shows a slightly lower TC than that taken for $LiGaSe_2$, K_z = 5.42 ± 0.27 W/mK vs. 6.3 ± 0.3 W/mK. Gallium is smaller than indium, 69.7 g/mol

vs. 114.8 g/mol, leading to a higher vibrational frequency and thus faster phonon transport as supported by Isaenko's study [36]. Therefore, the results of this study agree with theory and give a reasonable TC when comparing the two materials. Figure 12 below gives a visual comparison of the TCs of both materials in single crystal form.

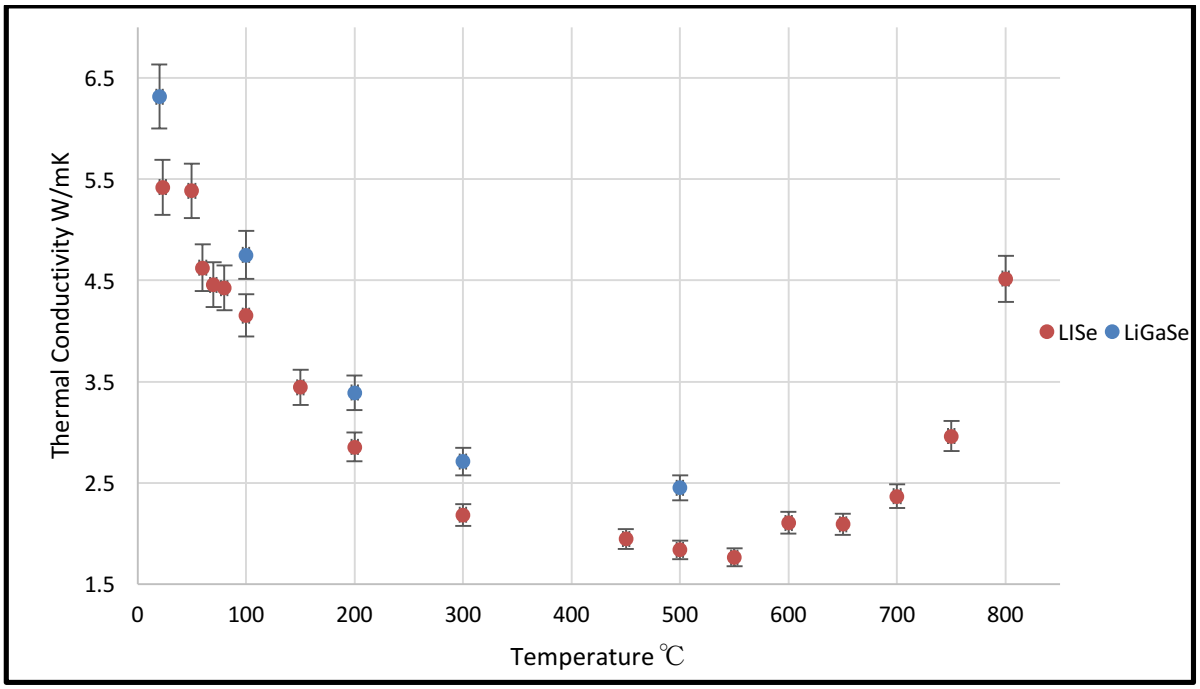

Figure 12: $LiGaSe_2$ and $LiInSe_2$ vs. Temperature

$LiIn_{1-x}Ga_xSe_2$ Pressed Pellets

The $LiIn_{1-x}Ga_xSe_2$ TC was measured in the same fashion as the $LiInSe_2$ pressed pellet samples. Once again the results showed an increase in TC after annealing. The TC for each composition vs. temperature is given in Figure 13 below. The trend does not show a coherent correlation between TC and an increase in Ga substitution. This behavior seems to go against the literature. Increased gallium concentration should promote faster movement of phonons through the material and thus increase the TC. Figure 13 clearly shows a sharp decrease in TC from 5% to 40% Ga substitution in place of In. The TC does increase with Ga concentration above 40% as seen in the 95% data. It is possible that vibrational modes of In and Ga are not on the same frequency and prevent uniform

phonon flow and thus cause a decrease in the TC. It is interesting that the pellets with the 95% In have a higher TC than their counterparts with 95% Ga. This goes against the theory based on vibrational frequency and ease of phonon transport. The $LiGaSe_2$ pellets had a lower thermal conductivity than all but the 60/40 substitution. This is clearly in conflict with the crystal data.

It is most likely that these results are not truly representative of the ideal case. It would be difficult to use this data to extract meaningful values for their single crystal counterparts. It is possible that annealing removed too much material in the samples containing gallium and that a lower annealing temperature could produce better results. While this is discouraging it does give a basis for experimental methodology in future experiments.

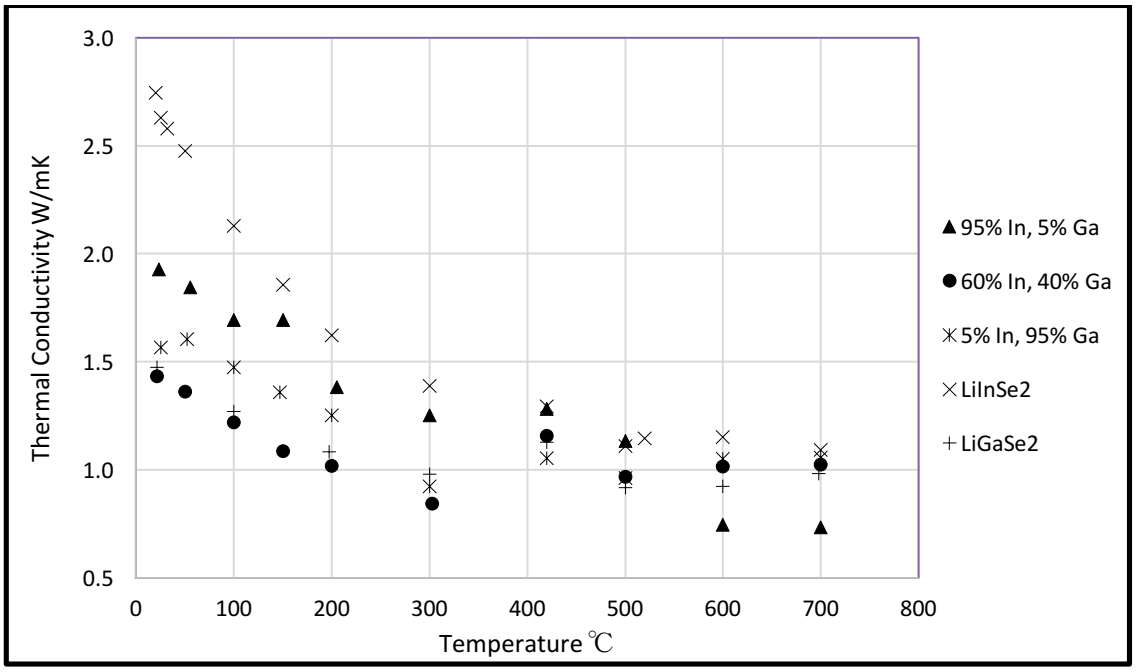

Figure 13: Comparison of $LiIn_{1-x}Ga_xSe_2$, $LiInSe_2$, and $LiGaSe_2$ pressed pellet thermal conductivity

All of the TC measurements showed a strange divergence from the established trend at 420 °C. This trend is present regardless of material composition or physical state, single vs. polycrystalline. The nickel circuit within the sensors undergoes a curie

transition between 300 and 420 °C making the thermal coefficient of electrical resistivity unreliable. It is highly likely that the variability in temperature is preventing the nickel from stabilizing and causing the electrical resistivity of the circuit to also be unstable. Therefore, the data should be analyzed without using the 420 °C data point.

Coefficient of Linear Thermal Expansions (CLTE)

Measurements on the Z-Axis

The CLTE was measured up to 500 °C at a temperature ramp rate of 5 °C/min. The results of that experiment are given in Figure 14 below. The material shows the same trend during both heating and cooling, meaning the material is structurally coherent through both phases.

The jumps in length between 0 and 50 minutes were shown to be a systematic error caused by the lab door opening and closing. These spikes do not impact the overall result and have been excluded from analysis. The figure clearly shows an acceleration in the material expansion near the maximum of the curve.

A closer look at the data during temperature increase is plotted in Figure 15 vs. temperature to give a better illustration of the accelerative behavior as a function of temperature. The top line is during temperature increase while the bottom is during cool down. Further data analysis pinpoints the change in the CLTE at just above 476 °C.

As discussed in earlier sections on TC, this temperature corresponds to the atomic bonds of Se being broken. Thus the increased expansion is likely due to Se dissociation from the lattice. The expansion is very linear up to 476 °C with an R^2 value of 0.9968. Therefore, we can confidently apply a stable CLTE value of $1.22 \pm 0.03 \times 10^{-5}$ K^{-1} from room temperature to 476 °C. The linearity of that region is shown visually in Figure 16 below. The red dotted line is the linear trend line of the data and follows the equation in the bottom right corner.

The obvious discontinuities in the figure were, once again, shown to be due to vibrational motion from opening and closing the laboratory door. Therefore, in the optimized experiment we would expect the expansion to be even more linear along this temperature regime with variations only due to crystalline defects within the lattice.

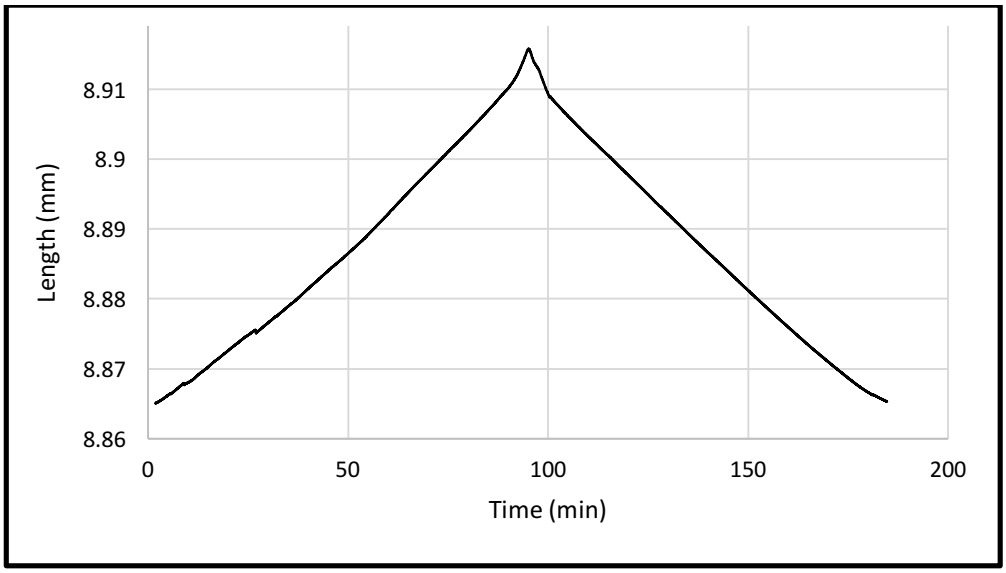

Figure 14: Sample length vs. time

The increased rate of expansion seen in Figure 14 and Figure 15 has been isolated and analyzed in Figure 17 below. The red dotted line is the linear trend line of the data and follows the equation in the bottom right corner. The expansion is happening at an accelerated rate in this region resulting in a much higher CLTE value of $3.68 \pm 0.18 \times 10^{-5}$ K^{-1}. This represents a 197% increase in the CLTE.

Measurements on the X and Y axis

The *x* and *y* axes were not predetermined before these experiments. The experiments showed very uniform expansion and then contraction in similar fashion to the measurements on the *z* axis. Figure 18 shows the expansion over the temperature gradient from room temperature to 500 °C. These figures show a much more uniform gradient due to elimination of discontinuities caused by the laboratory door closing.

It is also linear, $R^2 = 0.9997$, for the majority of the temperature gradient with the exception of the asymptotic behavior displayed over the last 50 degrees. Figure 19 gives a better view of the transition to nonlinear behavior.

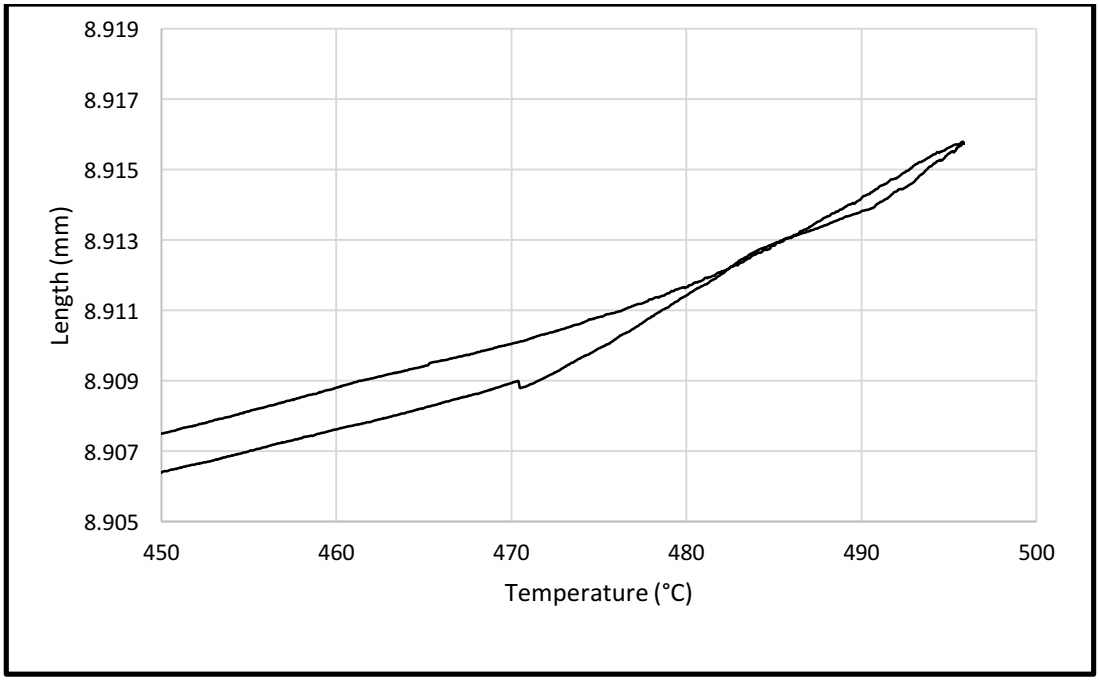

Figure 15: Sample Length vs. Temperature for the z-axis of $LiInSe_2$.

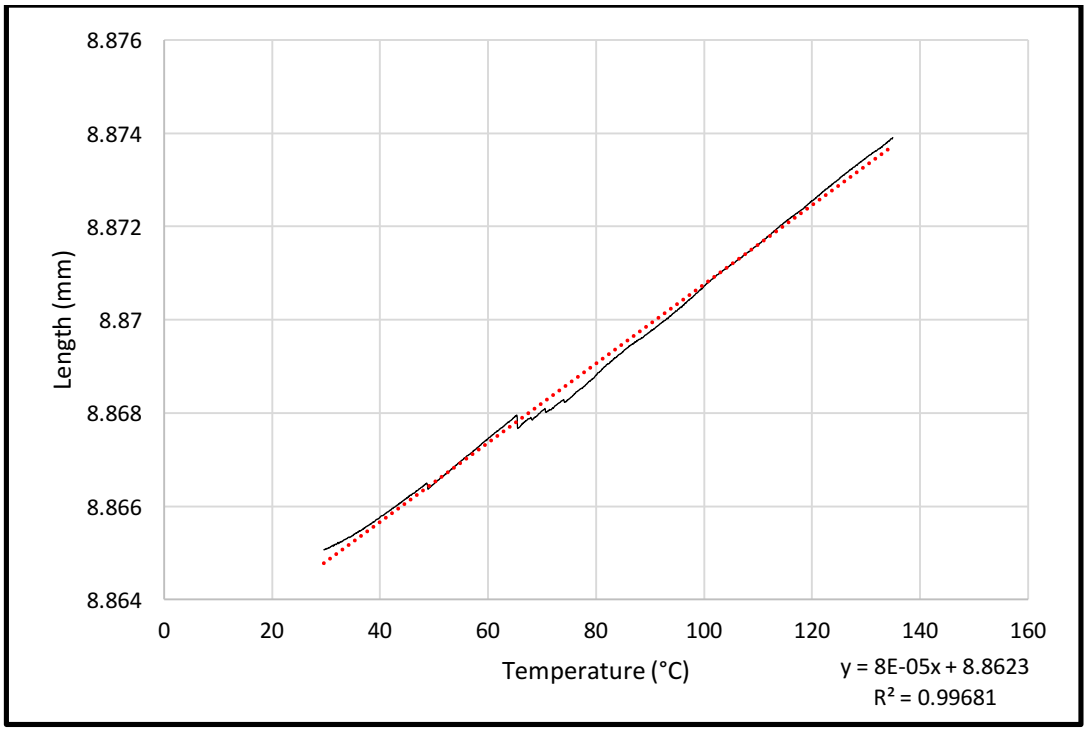

Figure 16: Linear region of expansion for $LiInSe_2$

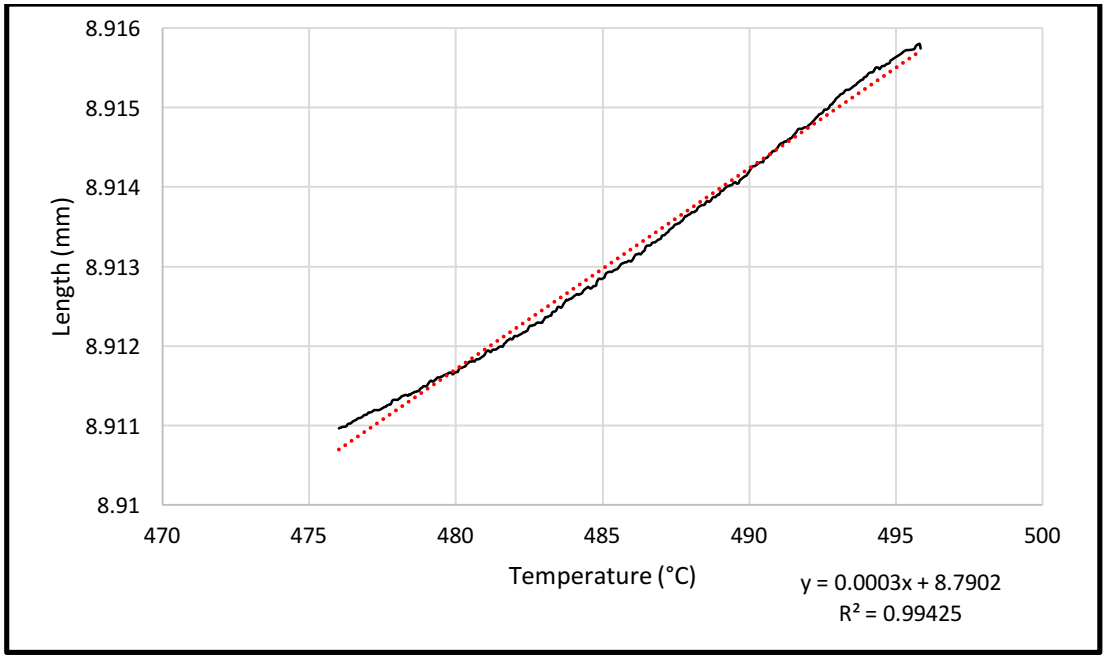

Figure 17: Accelerated region of expansion in $LiInSe_2$.

Further data analysis reveals that the change in expansion rate occurs at just over 455 °C. This change is both 20 °C lower and inverse of the change exhibited along the z axis. The CLTE for the y axis along the linear portion of expansion was found to be 1.13 ± 0.06 x 10^{-5} K^{-1}.The *x* axis was measured last and the crystal's expansion from room temperature to 500 °C is given in Figure 20 below.

It is not as linear as the *y* axis but is still very linear with an R^2 value of 0.9985. The CLTE of the *x* axis was found to be 1.32 ± 0.07 x 10^{-5} K^{-1}. A quick comparison of CLTE for all three axes is given in Table 4 below. In an orthorhombic crystal system, we would expect all three CLTE values to be different as the atomic spacing varies along all three axes. Thus, these results align nicely with theory.

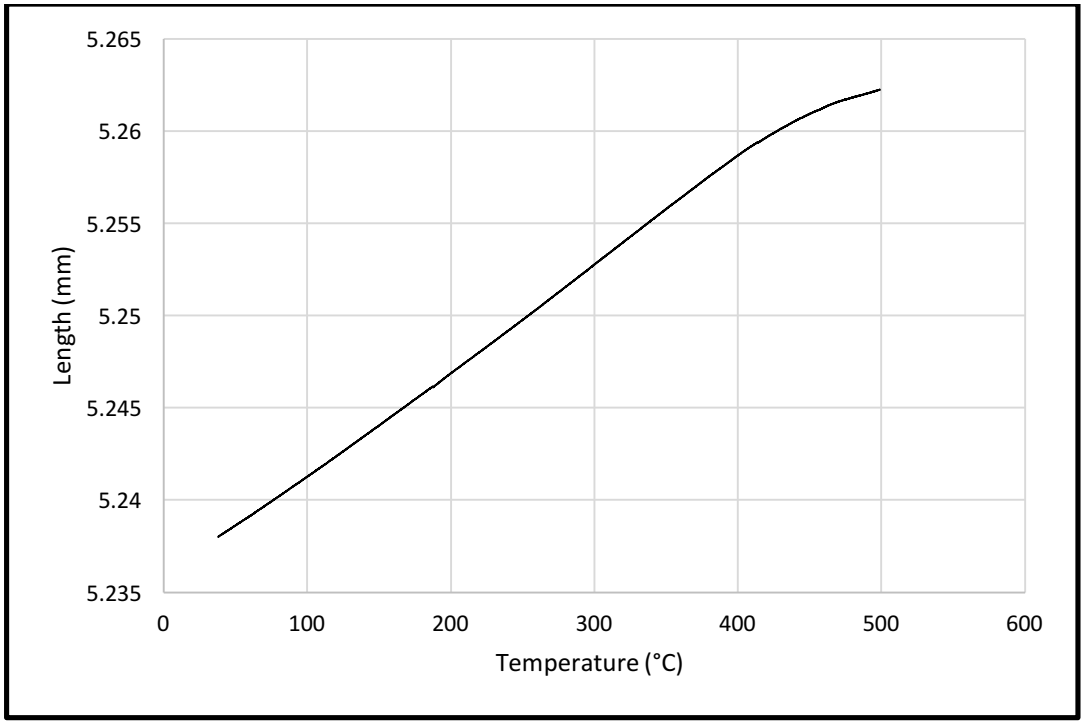

Figure 18: Length vs. Temperature for $LiInSe_2$ x axis.

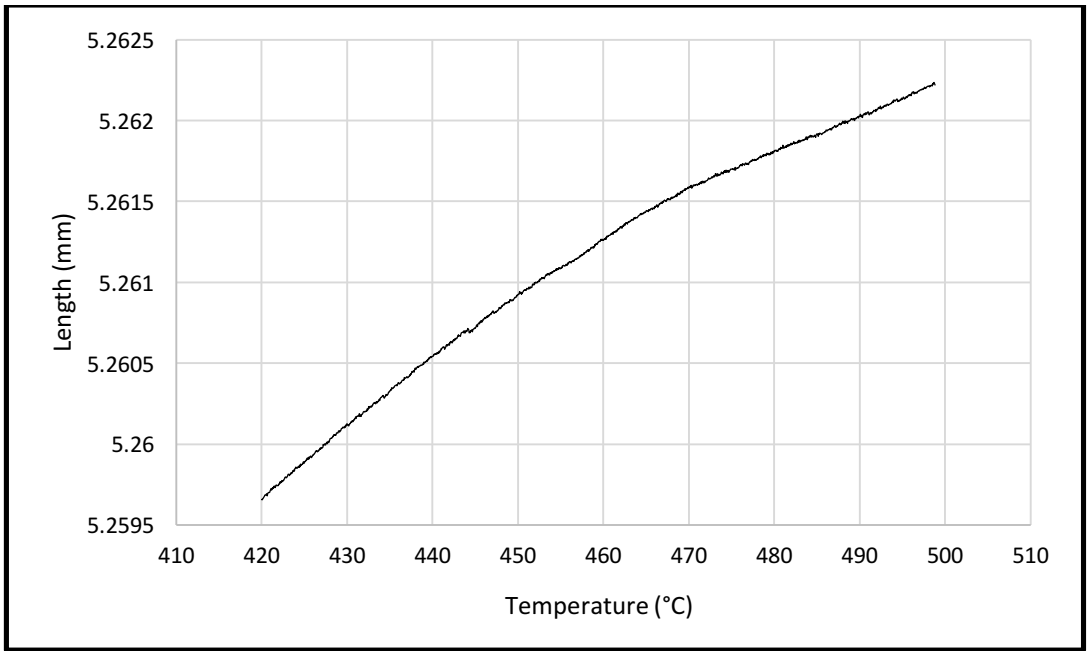

Figure 19: Acceleration of expansion in $LiInSe_2$ above 400 °C x axis.

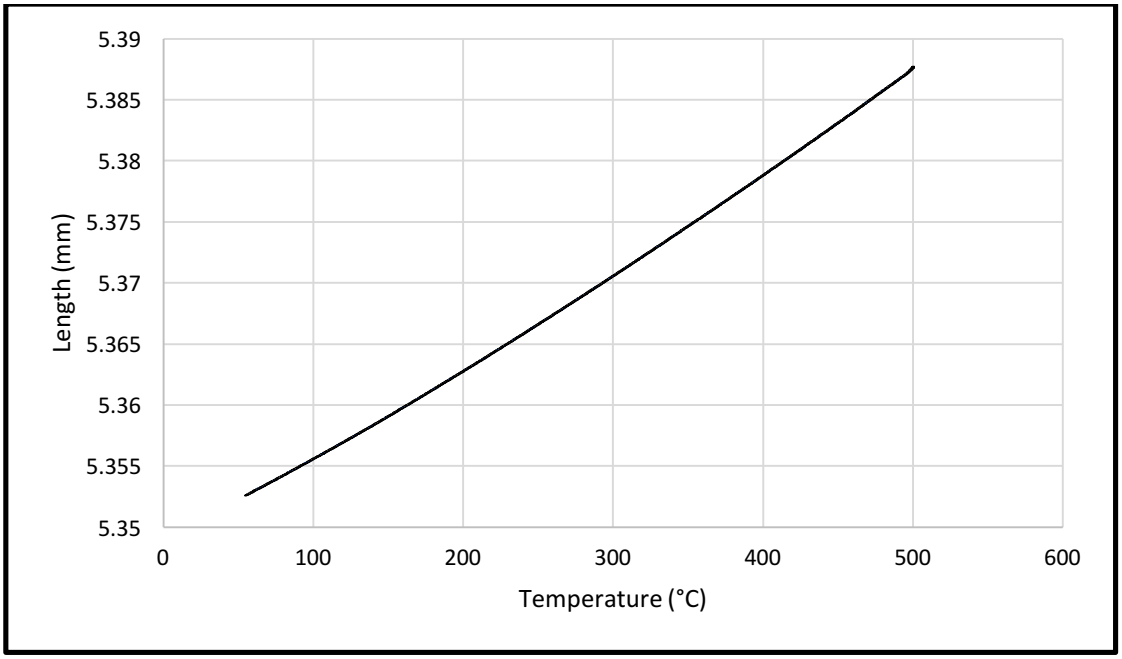

Figure 20: Thermal expansion of $LiInSe_2$ y axis.

Table 4: Axial CLTE comparison for $LiInSe_2$

	X	*Y*	*Z*
CLTE (K^{-1})	$1.32 \pm 0.07 \times 10^{-5}$	1.13 ± 0.06 x 10-5	$1.22 \pm 0.03 \times 10^{-5}$

Chapter 6

Conclusions and Recommendations

The results obtained were favorable and aligned with theory in nearly all areas investigated. The thermal conductivities of both $LiInSe_2$ and $LiGaSe_2$ single crystalline materials at room temperature are supported by pre-existing literature. However, high temperature measurements shown herein add to the body of understanding of Li-containing chalcogenides.

This research resulted in a reliable TC profile for $LiInSe_2$ from room temperature to 800 °C. The data shows a strong correlation to expected behavior based on previous experiments, theory, and known material properties. The TC decreases with temperature until the atomic bonds of Se are broken, at which point it rapidly increases.

It also investigated thermal properties of $LiIn_{1-x}Ga_xSe_2$ in pressed pellet form. This data showed very little correlation to the material composition. It is likely an inherent side-effect of the material composition. The $LiInSe_2$ pellet data resembles its single crystal counterpart much more than the $LiGaSe_2$. However, it would be difficult if not impossible to use pellet data to extrapolate values for single crystals; however, there are valuable lessons to be learned for future experiments of this nature.

The CLTE experiments provided insightful data along all three optical axes and can confidently be applied to future detector and crystal development. The CLTE was very linear with a very slight deviation from linearity in two of the three axial directions above 450 °C. The change in expansion rate is thought to be caused by phase transitions as the Se molecules begin breaking away from the lattice.

Future Work Needed to Develop Ideal Crystal

The immediate impact of this work lies in the opportunities available with existing computational models of crystal growth. The data acquired can be used to simulate various growth techniques and the resulting crystals. It will enhance current crystal growth models by adding a polynomial trend instead of a static number to describe thermal conductivity with respect to temperature. Through various cycles of growth simulation and calibration the optimum $LiIn_{1-x}Ga_xSe_2$ crystal can be achieved.

These studies should be couple with radiation response experiments to further the current project. The next major advancement will be finding a compromise between increased electron band gap from adding Ga and the neutron absorption limitations of higher In concentration. That crystal has the potential to be the best thermal neutron detection medium available on the market. With diligence, the effort could be accomplished in 3 to 5 years.

List of References

1. Knoll, G.F., *Radiation Detection and Measurement*. 4th ed, ed. D. Matteson. 2010, Hoboken, NJ: John Wiley and Sons Inc. . 830.
2. Richard T. Kouzes, J.H.E., Luke E. Erikson, Warnick J. Kernan, Azaree T. Lintereur, Edward R. Siciliano, Daniel L. Stephens, David C. Stromswold, Renee M. Van Ginhoven, Mitchell L. Woodring, *Neutron detection alternatives to 3He for national security applications.* Nuclear Instruments and Methods in Physics Research A, 2010(623): p. 1033-1045.
3. Stowe, A.C. *Investigation of a Novel 6LiInSe2 Detector for Neutron Transmission Imaging*. 2014. International Workshop on Radiation Imaging Detectors iWoRID.
4. Stowe, A.C., et al. *Lithium-containing semiconductor crystals for radiation detection*. in *MRS Online Proceedings Library*. 2013.
5. Munter, A. *Neutron Scattering Lenghts and Cross Sections*. 2013 January 7, 2013 [cited 2016 Febuary 1, 2016]; Available from: https://www.ncnr.nist.gov/resources/n-lengths/.
6. Richard T. Kouzes, A.T.L., Edward R. Siciliano, *Progress in alternative neutron detection to address the helium-3 shortage.* Nuclear Instruments and Methods in Physics Research A, 2014(784): p. 172-175.
7. Huang, K.-C., et al., *Scalable large-area solid-state neutron detector with continuous p–n junction and extremely low leakage current.* Nuclear Instruments and Methods in Physics Research Section A: Accelerators, Spectrometers, Detectors and Associated Equipment, 2014. **763**(0): p. 260-265.
8. Wiggins, B., et al., *Scintillation properties of semiconducting 6LiInSe2 crystals to ionizing radiation.* Nuclear Instruments and Methods in Physics Research Section A, Coming.
9. IAEA, *Safeguards Techniques and Equipment*, IAEA, Editor. 2011: Vienna.
10. Canberra, *Well Type neutron detector*. 2016.
11. Shah, K. *Hand-held Neutron Detector*. 2012 [cited 2016 February 22]; Available from: https://www.sbir.gov/sbirsearch/detail/385571.
12. Lejay, J. *Large CLYC:Ce and CLLB:Ce crystals for gamma neutron Detection systems*. Available from: http://www.crystals.saint-gobain.com/uploadedFiles/SG-Crystals/Documents/Technical/Large CLYC and CLLB crystals Poster-IEEE 2013.pdf.
13. U. Shirwadkar, J.G., E. Van Loef, *Investigating Scintillation Properties of Ce Doped CLYC.* IEEE, 2010: p. 1585-1588.
14. J. Glodo, R.H., K.S. Shah, *Development of CLYC Scintillator.* Journal of Crystal Growth, 2013(379): p. 73-78.
15. Luna Pellefri, E.B., *Performances of a 1"x1" Cs2LiYCl6 scintillator detector*. 2007.
16. Chad M Whitney, L.S.-P., Erik B. Johnson, *Gamma-neutron imaging system utilizing pulse shape discrimination with CLYC.* Nuclear Instruments and Methods in Physics Research, 2014(784): p. 346-351.
17. A. Giaz, F.C., *Thermal and fast neutron detection with two CLYC scintillators.* p. 95-200.

18. C.D. Bass, E.J.B., H. Breuer, C.R. Heimbach, T.J. Langford, J.S. Nico, *Characterization of a 6Li-loaded liquid organic scintillator for fast neutron spectrometry and thermal neutron detection.* Applied Radiation and Isotopes, 2013(77): p. 130-138.
19. Sanjoy Mukhopadhyay, H.R.M., *Portable gamma and thermal neutron detector using LiI(Eu) crystals*. Bechtel.
20. Isaenko, A.Y., S. Lobanov, A. Titov, V. Petrov, J.-J. Zondy, P. Krinitsin, A. Merkulov, V. Vedenyapin, J. Smirnova, *Growth and properties of LiGaX2 (X=S, Se, Te) single crystals for nonlinear optical applications in the mid-IR.* Crystal Research and Technology, 2002. **38**(3-5): p. 379-387.
21. T. J. Negran, H.M.K., and A. M. Glass, *Pyroelectric and Electrooptic Effects in LiIns2 and LiInSe2.* Pergamon Press, 1973. **8**: p. 743 - 748.
22. Zane W. Bell, D.A.C., S.S. Cristy, V. E. Lamberti, Arnold Burger, Brian F. Woodfield, Thomas Niedermayr, *Neutron Detection with cryogenics and semiconductors.* Physics Stat. Sol., 2005. **5**: p. 1592-1605.
23. Tupitsyn, E., et al., *Single crystal of LiInSe2 semiconductor for neutron detector.* Applied Physics Letters, 2012. **101**(20): p. 202101.
24. Jean-Jacques Zondy, V.P., Ludmila Isaenko, Alexander Yelisseyev, Olivier Bidault, *Optical, Thermal, Electrical, Damage, and Phase-Matching Properties of Lithium Selenoindate.* Optical Society of America, 2011.
25. Tupitsyn, E., et al., *Lithium containing chalcogenide single crystals for neutron detection.* Journal of Crystal Growth, 2014. **393**.
26. Wiggins, B., et al. *Investigation of non-uniformity and inclusions in 6LiInSe2 utilizing laser induced breakdown spectroscopy (LIBS)*. in *SPIE*. 2013. San Diego, CA: SPIE.
27. Eric Lukosi, E.H., Ashley C. Stowe, Robert Milburn, Dylan Richardson, Brenden Wiggins, Arnold Burger, Louis Santodonato, Hassina Bilheux, *Investigation of a Lithium Indium Diselenide Detector for neutron transmission imaging.* SPIE, 2014. **9213**(92130D).
28. Lukosi, E., *Response Functions of Semiconduction Lithium Indium Diselenide.* Nuclear Instruments and Methods in Physics Research, 2015.
29. N. D'Olympia, P.C., C.J. Lister, J. Glodo, R. Hawrami, K. Shah, U. Shirwadkar, *Pulse-shape analysis of CLYC for thermal neutrons, fast neutrons and gamma-rays.* Nuclear Instruments and Methods in Physics Research A, 2013. **715**: p. 121-127.
30. Cui, Y., et al., *Defects in 6LiInSe2 neutron detector investigated by photo-induced current transient spectroscopy and photoluminescence.* Applied Physics Letters, 2013. **103**(9): p. 092104.
31. Ashley C. Stowe, J.C., Pijush Bhattacharya, Eugene Tupitsyn, Brenden Wiggins, Michael Groza, Arnold Burger, *Lithium-containing semiconductor crystals for radiation detection.* Materials Research Society, 2013. **1576**.
32. Alan Ownes, A.P., *Compound Semiconductor Radiation Detectors.* Nuclear Instruments and Methods in Physics Research A, 2004(531): p. 18-37.

33. Jeffrey J. Derby, A.Y., *Bulk Crystal Growth of Electronic, Optical and Optoelectronic Materials*. Vol. 1. 2005: John Wiley and Sons. 574.
34. A. C. Stowe, J.S.M., P. Bhattacharya, E. Tupitsyn, A. Burger, *Synthesis of a potential semiconductor neutron detector crystal LiGa(Se/Te)2: Materials urity and compatibility effects.* SPIE, 2011. **8142**(81421H-1).
35. G. S. Nolas, J.Y., H. J. Goldsmith, *Thermal Conductivity: Theory, Properties, and Applications*. 1 ed. Physics of Solids and Liquids, ed. T.M. Tritt. Vol. 13. 2012, New York: Plenum Publishers. 306.
36. L. Isaenko, A.Y., S. Lobanov, P. Krinitsin, V. Petrov, J.-J. Zondy, *Ternary Chalcogenides LiBC2 (B = In, Ga; C = S, Se, Te) for mid-IR nonlinear optics.* Journal of Non-Crystalline Solids, 2006. **352**: p. 2439 - 2443.

Vita

Dustin C. Giltnane obtained an undergraduate degree from the University of Tennessee in Nuclear Engineering graduating in the class of May, 2014. He worked as a coop student at TVA during his undergraduate studies, helping in the development of a construction permit application in support of the Clinch River Small Modular Reactor Project. His primary job function was licensing documentation development and plant design reviews. That work lasted from September of 2011 through August of 2014. At which time he began working towards a master's degree. His undergraduate senior design project was to develop an alloy that could be used to coat spent fuel before being moved into long term dry cask storage. His team developed a 60/40 zinc/cadmium alloy and successfully bonded the alloy to zircalloy tubing. The project was chosen to represent the nuclear engineering program at the National ANS student design competition where the team was awarded 2nd place.

He went on to pursue a dual MBA/MS Nuclear Engineering immediately after completing his undergraduate work. He graduated from the MBA program in December, 2015. Throughout both programs he has worked as a graduate research assistant at CNS Y-12 in the development division. There he has conducted all the research outlined in this thesis and plans to continue working there as a full time employee in upon completion of the MS Nuclear Engineering degree. He expects to start work in the development division and later transition to the safeguards division.

Dustin's long term career goals include working to prevent the proliferation of Nuclear weapons and related components. To that end and as a part of his career Dustin plans on working with the IAEA and the NNSA on international counter-terror efforts abroad.